

PACS numbers: 81.07.Bc; 81.16.Mk
DOI: 10.1070/QE2010v040n11ABEH014441

Choice of a target with metal coating for laser-induced transfer of ultradispersed materials

T.V. Kononenko, M.A. Kamalov, A.F. Popovich, V.I. Konov, M. Sentis

Abstract. **The ejection of ultradispersed diamond from a metallised target surface irradiated by nano- and subnanosecond laser pulses is experimentally investigated. Several targets with different transparent bases (quartz, polymethylmethacrylate) and absorbing metal coatings (titanium, aluminium) are investigated. The effect of the metal layer thickness and pulse width on the range of energy densities in which the ejection of diamond nanopowder is due to the transverse strain of metal layer is analysed. The heating of the target rear surface from which transfer occurs, in dependence of the target and laser pulse parameters, is estimated.**

Keywords: *laser-induced transfer, nanopowders.*

1. Introduction

Currently, laser-induced forward transfer (LIFT) is the most promising alternative to such recognised techniques for forming thin-layer surface microstructures as contact and jet microprinting. Laser transfer combines flexibility, high spatial resolution, and universality; i.e., it can be applied to many urgent nano- and biomaterials. During the last ten years, numerous studies have convincingly demonstrated a very wide range of applications of this method: from formation of various elements for microelectronics devices based on metal and multicomponent nanopowders [1 – 4] and polymers [5, 6] to design of biosensors; biochips; and complex structures based on proteins [7, 8], DNA [9, 10], and living cells [7, 8, 11].

Various versions of buffer layers are widely used to reduce the thermal and radiative effect of laser radiation on the material transferred. Possible types of buffer are a thin metal [12, 13] or polymer [3, 5] film located between the transferred material and thick transparent base, as well as a liquid matrix [1, 4, 7, 8], in which the transferred material is uniformly distributed. The target is irradiated from the side of the base, and the main material is ejected from its surface as a result of complete or partial evaporation of the buffer, which is also transferred to the substrate. However, the buffer layer can be used in another way. The parameters of the metal [14, 15] or polymer [16] film, as well as the irradiation conditions, can be chosen so as to make the film remain on the target but undergo short-term local blistering under laser irradiation to provide ejection of the main material from the target.

Important advantages of blistering laser transfer are its absolute purity (i.e., it is only the main material that is transferred), applicability for solid and liquid materials, and effective isolation of the material transferred from heating by laser pulses (using a sufficiently thick buffer). In our opinion, metal buffer layers have certain technological advantages in comparison with polymer ones: existence of developed techniques for deposing metal films on large areas, absence of special requirements for the radiation wavelength, and more convenient control of the transfer process.

In our first experiments [14] blistering was initiated by fairly short (50 ps) laser pulses; however, subsequent experimental studies [15] showed that in principle longer (nanosecond) pulses can also be used. This result is of practical importance, because nanosecond laser systems are widespread: from solid-state (IR and visible) lasers to excimer (UV) laser systems, which provide a high spatial resolution. Unfortunately, an evident consequence of applying longer laser pulses is deeper penetration of thermal wave into the metal coating, as a result of which the material transferred is more heated. This problem can be solved by increasing the metal coating thickness. However, this approach has a limitation: according to the existing experimental data [15], an increase in the coating thickness is accompanied by successive narrowing of the intensity range where blistering can be implemented.

The purpose of this study was to analyse the possibilities of controlling the liquid-free laser transfer in the blistering regime by varying the target parameters. We experimentally investigated the ejection of ultradispersed diamond (UDD) from different targets under irradiation by nanosecond and subnanosecond IR pulses. Targets differed by the materials of substrate (quartz, polymer) and metal coating (titanium, aluminium) and by the metal film thickness. The range of laser energy densities where blistering transfer could occur was measured for each target and the degree of heating of the target rear surface, which was in contact with the material transferred, was estimated by numerical simulation.

T.V. Kononenko, M.A. Kamalov, A.F. Popovich, V.I. Konov A.M. Prokhorov General Physics Institute, Russian Academy of Sciences, ul. Vavilova 38, 119991 Moscow, Russia; e-mail: kononen@nsc.gpi.ru
M. Sentis LP3 Universite Aix-Marseille II, Luminy, Case 917, 13288 Marseille Cedex 9, France

Received 19 August 2010; revision received 18 October 2010
Kvantovaya Elektronika **40** (11) 1034 – 1040 (2010)
Translated by Yu.P. Sin'kov

2. Experimental

The transparent bases of targets were polished plates of fused silica and polymethylmethacrylate (PMMA), onto which a thin titanium or aluminium film was deposited by vacuum evaporation. The thickness of the metal film was varied from 50 nm to 1.2 – 1.7 μm. Deposition of titanium films thicker than 200 – 300 nm on PMMA substrates met serious difficulties because of the substrate superheating and deformation. Thus, we performed a comparative study of laser transfer for targets of three types: quartz/titanium, quartz/aluminium, and PMMA/aluminium.

The ultradispersed diamond obtained by explosion was placed in distilled water with a dissolved surfactant (sodium dodecyl sulfate, 2.0 mg mL^{-1}). To exclude formation of large diamond particles (agglomerates), the suspension was subjected to ultrasonic treatment with subsequent sedimentation. Then it was distributed as a thin layer over the metallised target surface, and, after the water evaporation, a layer of diamond nanoparticles ~ 1 μm thick was formed on the target surface. According to the atomic force microscopy data, the particle diameter did not exceed 200 nm.

Laser pulses 500 ps and 7 ns wide were generated by a tunable solid-state Nd : YAP laser ($\lambda = 1078$ nm), operating in the active mode locking and Q-switched regimes, respectively. The maximum spread in energy from pulse to pulse at a repetition rate of 5 Hz was ±10 %. Experiments were performed in air at normal atmospheric pressure. Laser radiation was focused through the transparent base on the metal film on the target surface into a spot about 30 μm in diameter (at the level of 1/e). Each target under study was irradiated with single pulses of different energy, and the irradiated samples were investigated with an optical microscope.

The sizes of the region of diamond particle ejection and the region where the metal layer was completely removed were determined for the rear side of the irradiated target. The incident energy density at the boundary of each region was calculated based on the known size of the laser radiation spot. A significant decrease in the 'boundary' energy density with an increase in the laser pulse energy was observed in most cases. This effect is likely to be caused by the generation of a surface acoustic wave (SAW), which propagates from the centre of the laser spot to its periphery and transfers an additional normal acceleration to the free metal surface. As a result the powder can be ejected from the target surface (or the metal layer can be removed) at a relatively low local energy density at the periphery of the laser spot. The size of the SAW-affected region increases with an increase in the laser pulse energy and may significantly exceed the irradiated spot size. For example, in [17], where the laser-induced SAW was investigated microparticles were removed from the target surface on an area of ~ 1 cm^2, while the laser spot diameter was about 15 μm. In our experiments the thresholds for nanoparticle ejection and metal layer removal were found for each target; they were determined as the limiting energy densities at the boundary of the corresponding region at the region size tending to zero. The thus found parameters characterise the local laser effect.

Sometimes the microscopic study of the irradiated targets from the side of the transparent base revealed bright spots with a sharp contour at the base/metal interface. This effect was interpreted as local peeling of the metal film from the substrate. Indeed, the total reflection coefficient of the two newly formed interfaces [quartz/vacuum (R_1) and vacuum/metal (R_2)] should exceed the reflection coefficient of the initial metal/quartz interface (R_3): $R_1 + R_2 > R_3$. For example, in the case of titanium coating these parameters (for $\lambda = 540$ nm) are $R_1 = 0.035$, $R_2 = 0.495$ and $R_3 = 0.382$. The newly formed bright spot was retained with an increase in the energy density up to complete removal of metal from the target, which was generally preceded by metal film cracking and occurrence of a visible gap between the metal and base. The minimum necessary energy density was determined for each peeling case; to this end, the size of the peeling region was measured for different pulse energies.

3. Simulation of target heating

In our experiments the characteristic size of irradiated region greatly exceeded the thermal diffusion length during the laser pulse in both the metal film and transparent base. Therefore, the dynamics of change in the target temperature can be described by the one-dimensional heat-conduction equation

$$\frac{\partial T}{\partial t} = \frac{1}{\rho C(T)} \frac{\partial}{\partial z} \left[K(T) \frac{\partial T}{\partial z} \right] + \frac{\alpha I(z,t)}{\rho C(T)}, \quad (1)$$

where T is temperature; and ρ, $C(T)$, $K(T)$ and α are, respectively, the local density, specific heat, thermal conductivity, and the optical absorption coefficient of the metal. The spatial and temporal dependence of the laser intensity in the metal layer was determined as

$$I(z,t) = I_0(t)(1 - R)\exp(-\alpha z), \quad (2)$$

where $I_0(t)$ is the time intensity profile, approximated by the Gaussian distribution; R is the sample reflection coefficient; and z is the distance from the metal/substrate interface.

The temperature profiles were calculated by the finite-difference method taking into account the temperature dependences of the thermophysical properties [$C(T)$ and $K(T)$] of the substrate and metal coating. The presence of diamond powder on the target was disregarded; i.e., the heat flux at the metal/diamond interface was assumed to be zero. The melting and evaporation fronts were not explicitly selected; however, the necessary expenditure of energy to the phase transitions in the metal layer was taken into consideration. The possibility of thermal decomposition of quartz at $T > 3070$ K [18] or PMMA at $T > 460 - 550$ K [19] was neglected in the calculations. The change in the optical properties of metals upon heating and melting was also disregarded.

The thermal and optical parameters of the target are generalised in Table 1 [20 – 24]. It was assumed that the metal at the interface with the transparent base begins to evaporate after reaching the boiling temperature and absorption of necessary amount of heat (see Table 1). Based on this assumption, we determined the threshold laser energy density that causes metal evaporation.

4. Measurement results and discussion

The experimentally measured thresholds for diamond nanopowder ejection and local removal of metal layer for the quartz/titanium, quartz/aluminium, and PMMA/

Table 1.

Parameters of target components	Titanium	Aluminium	Quartz	PMMA
Melting temperature/K	1941	933		
Boiling temperature/K	3533	2793		
Latent heat of melting/J cm^{-3}	1.46×10^3	1.08×10^3		
Latent heat of evaporation/J cm^{-3}	4.20×10^4	2.93×10^4		
Density/g cm^{-3}	4.51	2.69	2.2	1.19
Thermal conductivity/W m^{-1} K^{-1}	$14.26 + 6.82 \times 10^{-3}T$	$231 + 4.65 \times 10^{-2}T - 7.64 \times 10^{-5}T^2$ ($T < 933K$), $39.2 + 7.34 \times 10^{-2}T - 2.12 \times 10^{-5}T^2 + 1.61 \times 10^{-9}T^3$ ($T > 933$ K)	$8.22 \times 10^{-14}T^5 - 7.54 \times 10^{-10}T^4 + 2.6 \times 10^{-6}T^3 - 4.26 \times 10^{-3}T^2 + 3.57T - 28.16$	0.19
Specific heat/J kg^{-1} K^{-1}	$479 + 0.18T$	$755.4 + 0.477T$ ($T < 933$ K), 1176.8 ($T > 933$ K)	$1.15 + 7.57 \times 10^{-4}T$	1.32×10^3
Absorption coefficient/cm^{-1}	3.9×10^5	1.2×10^6		
Reflectance	0.43	0.93		

aluminium targets with metal layers of different thickness are presented in Figs 1, 2, and 3, respectively, which show the effect of 500-ps or 7-ns laser pulses. In addition, the experimental data on the minimum energy density at which local peeling of metal coating from the transparent base occurs are given.

The threshold energy densities that initiate evaporation of metal at the interface with the base (according to the results of numerical simulation of the laser heating of target) are also given for the quartz-base targets (Figs 1, 2). These evaporation thresholds almost coincide with the metal peeling thresholds in the cases where peeling was experimentally observed. At the same time, for all the targets that did not exhibit metal peeling (i.e., the corresponding bright circles were absent), the calculated threshold for metal evaporation exceeded the threshold for metal removal from the target. This indicates that the metal layer is removed before the evaporation onset; therefore, its local peeling cannot be observed. Removal occurs without evaporation due to the through melting of the metal layer, as evidenced by the results of numerical simulation. The good correspondence between the experimental and calculated data verifies the computational regimel used and unambiguously establishes the nature of metal peeling.

The dependences of the thresholds of nanoparticle ejection and metal layer fracture on the layer thickness limit (from two sides) the range of parameters (metal thickness and energy density) in which 'pure' nanopowder transfer in the blistering regime may occur. For the quartz-base targets (see Figs 1, 2) the evaporation curve divides this range into two parts. Below this curve the motion of the metal surface, which provides diamond powder ejection, is caused only by the laser-induced thermal expansion of the target (mainly the metal film). According to our estimate, which is based on the results of numerical simulation of the temperature profile in the target and the data on the

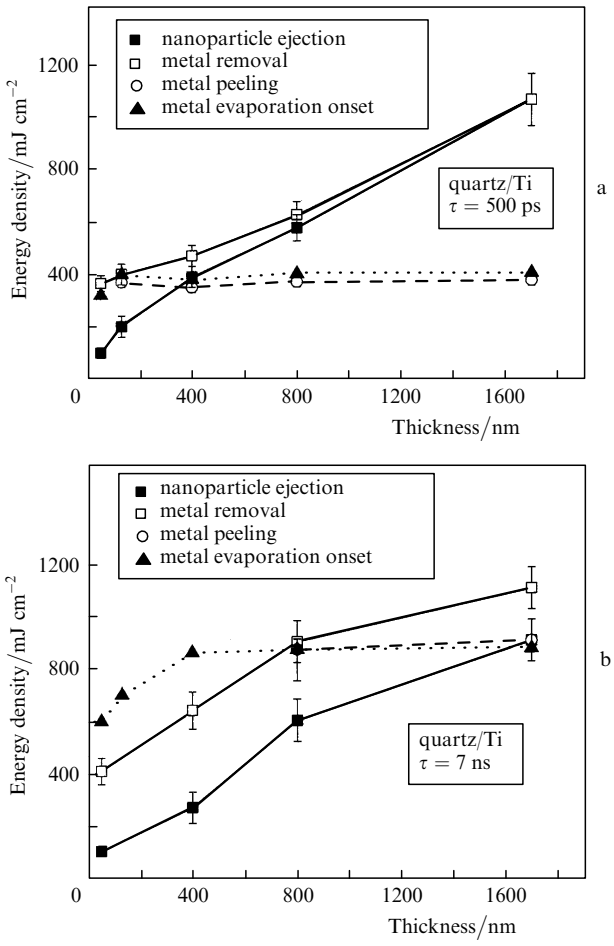

Figure 1. Dependences of the threshold energy density on the metal layer thickness for the quartz/titanium target irradiated with (a) 500-ps and (b) 7-ns pulses.

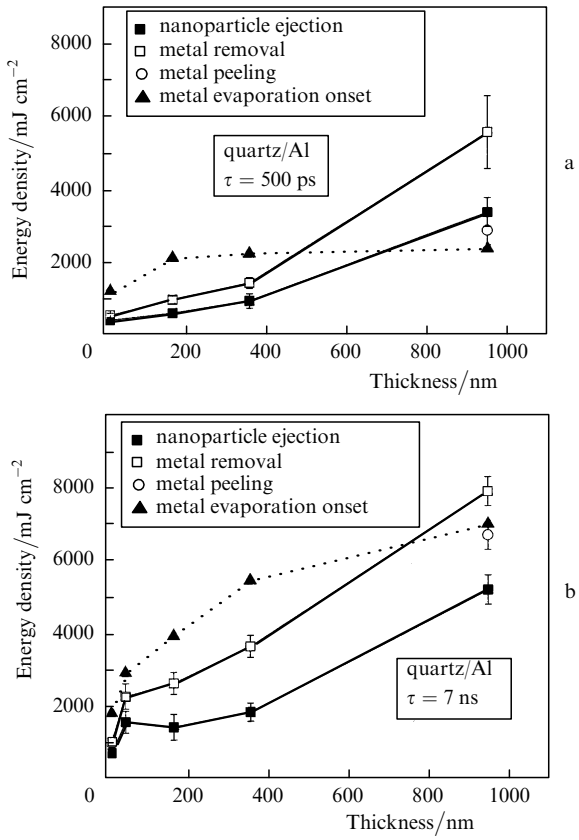

Figure 2. Dependences of the threshold energy density on the metal layer thickness for the quartz/aluminium target irradiated with (a) 500-ps and (b) 7-ns pulses.

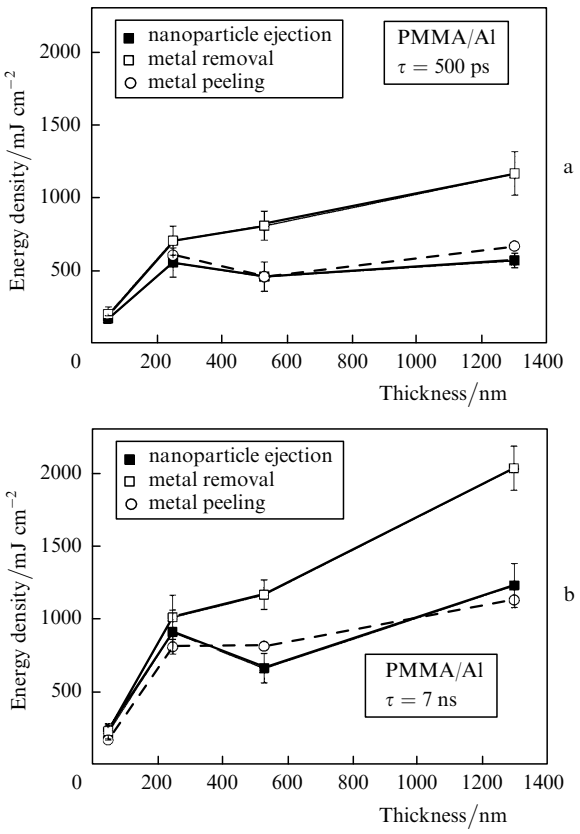

Figure 3. Dependences of the threshold energy density on the metal layer thickness for the PMMA/aluminium target irradiated with (a) 500-ps and (b) 7-ns pulses.

coefficients of linear thermal expansion of titanium ($\alpha = 1.6 \times 10^{-5}$ K^{-1} at $T < 1941$ K and $\alpha = 3.9 \times 10^{-5}$ K^{-1} at $T > 1941$ K [22]) and quartz ($\alpha \sim 5 \times 10^{-7}$ K^{-1} [25]) at a laser energy density of 250 mJ cm^{-2} on the target, the maximum increase in the thickness of 50-nm titanium layer is 4.4 nm, whereas the quartz base expands by only 0.2 nm. With an increase in the titanium layer thickness, the absolute values of the thermal expansion of the metal and quartz increase and decrease, respectively.

For thin metal layers thermal expansion is the only mechanism responsible for the acceleration and ejection of diamond powder. However, with an increase in the metal layer thickness the efficiency of the thermal deformation mechanism reduces, as evidenced by the gradual increase in the ejection threshold. The excess of the ejection threshold above the metal evaporation (peeling) threshold indicates that blistering transfer becomes impossible without the formation of a bubble filled with hot vapour at the base/metal interface. Obviously, when considering the parameter range above the evaporation curve, one must take into account not only the thermal expansion of the metal layer but also its motion as a whole, caused by the expanding vapour.

The calculated metal evaporation curve is an important reference, which allows one to estimate more exactly the effect of experimental conditions on the ejection and metal removal thresholds. For example, the increase in the pulse width from 500 ps to 7 ns is accompanied by a significant decrease in both thresholds with respect to the evaporation curve, although the absolute thresholds change only slightly. Apparently, the initial reason is the increase in the characteristic propagation length of thermal wave during the pulse. On the one hand, this causes deeper melting of the metal layer and facilitates its removal, which becomes possible at lower temperatures at the base/metal interface. On the other hand, a thicker layer is subjected to thermal expansion, which increases the ejection efficiency and reduces the corresponding threshold energy density. Replacement of titanium with aluminium also decreases both thresholds with respect to the evaporation curve. At the same time, the threshold magnitudes significantly increase, mainly because of the large reflection coefficient of aluminium (see Table 1).

In this case, we can suggest a complex effect, caused by the change in the coating parameters. The decrease in the metal removal threshold is facilitated by both the larger thermal wave propagation length in aluminium due to its higher thermal conductivity ($K_{Al} = 237$ W m^{-1} K^{-1} $\gg$ $K_{Ti} = 16$ W m^{-1} K^{-1} at $T = 300$ K) and its lower melting temperature. The relative decrease in the ejection threshold can be explained by the enhancement of the thermal deformation, which is caused by heating the metal layer to a larger depth because of the high thermal conductivity of aluminium and its higher (in comparison with titanium) thermal expansion coefficient.

Replacement of a quartz substrate with a polymer one (Fig. 3) significantly affects all measured parameters. First of all, the calculated temperatures of aluminium film peeling from PMMA turned out to be much lower than the aluminium boiling temperature (2520 °C): for different

targets under study they were in the ranges of 550 – 750 °C (irradiation by 500-ps pulses) and 400 – 600 °C (7-ns pulses). This fact indicates that the metal layer peeling is caused by the thermal decomposition of the polymer substrate. It is known that upon slow (furnace) heating, the thermal decomposition of PMMA begins at 190 – 280 °C (depending on the production technology) and is completed at 350 – 400 °C [19]. One might suggest that the higher temperature threshold of thermal decomposition for forming a gas interlayer at the PMMA/aluminium interface, which was found in our calculations, is caused by the short time of laser heating (at a limited decomposition rate). This is evidenced by the aforementioned tendency of the calculated peeling temperatures to increase with a decrease in the laser pulse width from 7 to 500 ps. The second specific feature of the targets with a polymer substrate is the coincidence of the ejection threshold with the metal peeling threshold. This means that in all cases the powder ejection from the target is primarily due to the formation of a gas bubble.

Note that the ejection of microparticles from the target surface, which is caused by the thermal expansion of target surface layer under pulsed laser irradiation, was previously investigated by many researchers in terms of the problem of so-called dry laser cleaning (see, for example, [26, 27] and references therein). However, the data obtained in these studies cannot be directly compared with the results of our experiments even when both dry laser cleaning and blistering transfer are caused by the same thermal deformation mechanism. The main reason is the radically different design of the targets used for blistering transfer: in contrast to the uniform targets subjected to laser cleaning, they consist of two layers: a transparent base and an absorbing metal. Hence, in this case the consideration must performed with introduction of some new parameters that are important for blistering transfer, including the metal layer thickness and the removal threshold for this layer under laser irradiation. A comparison of the parameters that are common for the effects under consideration also suggests their qualitative difference. For example, it was experimentally shown and theoretically substantiated that the laser cleaning threshold significantly increases with an increase in the pulse width [26, 28]. However, in our experiments the thresholds of particle ejection from the target (at a fixed thickness of metal layer) were almost independent of the pulse width. Nevertheless, the approaches and methodology that were developed to analyse laser cleaning appear to be promising for studying the blistering transfer.

When comparing different target configurations and laser irradiation regimes from the point of view of maximum reliability and reproducibility of blistering transfer, it is expedient to use the concept of relative operating range of energy densities ΔF, which is determined by the expression

$$\Delta F = (F_{\text{rem}} - F_{\text{eject}} - \delta F_{\text{rem}} - \delta F_{\text{eject}})/F_{\text{eject}}, \qquad (3)$$

where F_{rem} is the threshold for metal layer removal; F_{eject} is the threshold for powder ejection from the target; and δF_{rem} and δF_{eject} are the spreads in measuring the corresponding thresholds. The δF_{rem} and δF_{eject} values are partly determined by the conventional error in measuring the experimental parameters (pulse energy, size of ejection or metal removal region); however, real fluctuations of ejection and removal thresholds at different points of the target make a larger contribution to these values. These fluctuations can be caused by microdefects on the substrate or film, nonuniform powder distribution over the target surface, etc. Note that the operating range can be negative (hatched area in Fig. 4) if the total spread of removal and ejection thresholds ($\delta F_{\text{rem}} + \delta F_{\text{eject}}$) exceeds the difference in their average values ($F_{\text{rem}} - F_{\text{eject}}$). In practice this means that the inequality $F_{\text{eject}} < F < F_{\text{rem}}$ (F is the current energy density) cannot be reliably implemented for multiple transfer at different points of the target. Moreover, in view of inevitable fluctuations of the laser pulse energy (± 10 % in our case), reliable pure transfer of the nanopowder from different points of the target could be implemented only at $\Delta F > 0.2$. According to the data in Fig. 4, the operating range for the targets with titanium coating systematically decreased with an increase in the coating thickness; thus, the condition $\Delta F > 0.2$ was satisfied for only targets with sufficiently thin titanium films. A reverse tendency was observed for targets with aluminium coating; correspondingly, targets with a thick metal layer were of practical interest in this case. The operating range for these targets somewhat expanded with an increase in the pulse width.

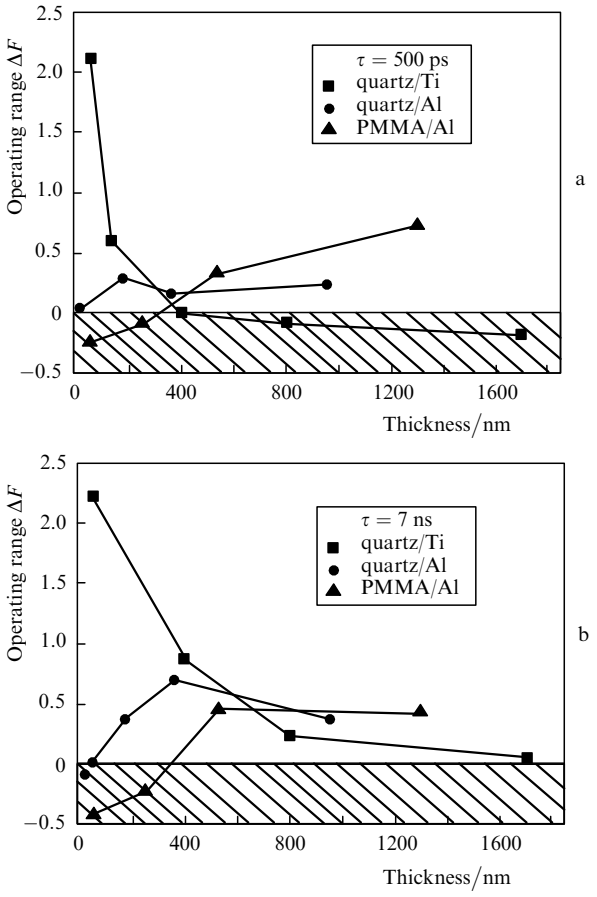

Figure 4. Relative width of the operating range of energy densities for the blistering regime. The pulse widths are (a) 500 ps and (b) 7 ns.

An additional factor that must be taken into account when choosing the optimal transfer conditions is the possible heating of the material transferred. In the first-order approximation one can assume that the free metal surface is accelerated until the maximum temperature is reached at the substrate/metal interface, after which slowing

down begins. Hence, the inertial powder ejection from the target is expected to occur approximately at the end of the laser pulse. The results of calculating the increase in the temperature of the metal film free surface, ΔT, at this instant for all targets satisfying the condition $\Delta F > 0$ are shown in Fig. 5. As was suggested, the expected heating temperature of transferred material varies in a wide range, decreasing with an increase in the metal film thickness.

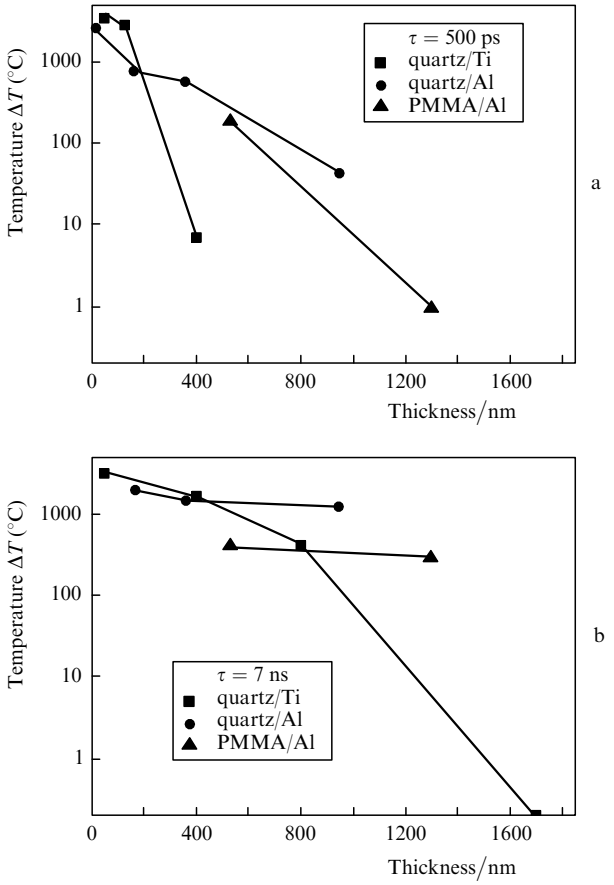

Figure 5. Temperature of the free surface of metal layer by the end of laser pulse. The pulse widths are (a) 500 ps and (b) 7 ns.

The 'safe' heating level of transferred material depends on its nature. For diamond nanopowder, as for most other inorganic materials, a short-term heating to 100–300 °C does not lead to any structural changes. For many organic materials the safe level is much lower: from 1 to 10 °C. Nevertheless, a comparison of Figs 4 and 5 allows one to draw justified conclusions about the prospects of practical application of targets of different types. In particular, targets with titanium coating do not appear promising for heat-sensitive materials, because heating with $\Delta T < 100$ °C can be implemented only for targets with a narrow operating range ($\Delta F < 0.2$). Irradiation of targets with aluminium coating by nanosecond pulses is also undesirable, because for different substrates the heating of the free metal surface is $\Delta T > 1000$ °C (quartz) or $\Delta T > 300$ °C (PMMA). An increase in the coating thickness to several micrometers cannot significantly improve the situation, judging from the slope of the corresponding curves in Fig. 5b. Shortening the laser pulse to 500 ps sharply decreases the heating temperature for both types of targets with aluminium coating. The PMMA/aluminium target demonstrates the best characteristics. At a metal layer thickness of 1.3 μm the relative operating range is $\Delta F = 0.7$, and the heating of the free metal surface does not exceed 1 °C. Moreover, proceeding from the tendencies observed, one would expect further improvement of both parameters with an increase in the coating thickness.

5. Conclusions

We demonstrated wide possibilities for controlling blistering laser transfer by changing the target parameters (substrate material, type of metal coating, and its thickness) and the laser pulse width. The choice of the target determines the relative operating range of energy densities in which nanopowder undergoes blistering transfer, as well as the mechanism of acceleration of the free metal surface and the degree of heating of particles before their ejection. Shortening of the laser pulse reduces its thermal effect on the material transferred. The comparison of targets of three types revealed the best combination of characteristics [i.e., maximum operating range ($\Delta F = 0.7$) with minimum heating of the material transferred ($\Delta T = 1$ °C)] for the PMMA/aluminium target irradiated with subnanosecond (500 ps) pulses.

Acknowledgements. This work was supported by the Federal Target Program 'Scientific and Scientific-Pedagogical Personnel of Innovative Russia' (state contract no. P951) and the Russian Foundation for Basic Research (Grant No. 10-02-93106).

References

1. Pique A., Chrisey D.B., Auyeung R.C.Y., Fitz-Gerald J., Wu H.D., McGill R.A., Lakeou S., Wu P.K., Nguyen V., Duignan M. *Appl. Phys. A*, **69**, S279 (1999).
2. Fitz-Gerald J.M., Pique A., Chrisey D.B., Rack P.D., Zeleznik M., Auyeung R.C.Y., Lakeou S. *Appl. Phys. Lett.*, **76**, 1386 (2000).
3. Xu J., Liu J., Cui D., Gerhold M., Wang A.Y., Nagel M., Lippert T.K. *Nanotechnology*, **18**, 025403 (2007).
4. Kim H., Auyeung R., Lee S., Huston A., Pique A. *Appl. Phys. A*, **96**, 441 (2009).
5. Fardel R., Nagel M., Nuesch F., Lippert T., Wokaun A. *Appl. Phys. Lett.*, **91**, 061103 (2007).
6. Rapp L., Diallo A.K., Alloncle A.P., Videlot-Ackermann C., Fages F., Delaporte P. *Appl. Phys. Lett.*, **95**, 171109 (2009).
7. Wu P.K., Ringeisen B.R., Callahan J., Brooks M., Bubb D.M., Wu H.D., Pique A., Spargo B., McGill R.A., Chrisey D.B. *Thin Solid Films*, **398-399**, 607 (2001).
8. Wu P.K., Ringeisen B.R., Krizman D.B., Frondoza C.G., Brooks M., Bubb D.M., Auyeung R.C.Y., Pique A., Spargo B., McGill R.A., Chrisey D.B. *Rev. Sci. Instrum.*, **74**, 2546 (2003).
9. Karaiskou A., Zergioti I., Fotakis C., Kapsetaki M., Kafetzopoulos D. *Appl. Surf. Sci.*, **208-209**, 245 (2003).
10. Serra P., Fernandez-Pradas J.M., Colina M., Duocastella M., Dominguez J., Morenza J.L. *J. Laser Micro/Nanoengineering*, **1**, 236 (2006).
11. Ringeisen B.R., Chrisey D.B., Pique A., Young H.D., Modi R., Bucaro M., Jones-Meehan J., Spargo B.J. *Biomaterials*, **23**, 161 (2002).
12. Hoppa B., Smausz T., Antal Zs., Kresz N., Bor Zs., Chrisey D. *J. Appl. Phys.*, **96**, 3478 (2004).
13. Rapp L., Cibert C., Alloncle A.P., Delaporte P. *Appl. Surf. Sci.*, **255**, 5439 (2009).
14. Kononenko T.V., Alloncle P., Konov V.I., Sentis M. *Appl. Phys. A*, **94**, 196 (2009).

15. Kononenko T.V., Nagovitsyn I.A., Chudinova G.K., Mihailescu I.N. *Appl. Surf. Sci.*, **256**, 2803 (2010).
16. Kattami N.T., Purnick P.E., Weiss R., Arnold C.B. *Appl. Phys. Lett.*, **91**, 171120 (2007).
17. Kolomenskii Al.A., Maznev A.A. *Piz'ma Zh. Eksp. Teor. Fiz.*, **53**, 403 (1991).
18. Schick H.L. *Chem. Rev.*, **60**, 331 (1960).
19. Sazanov Yu.N., Skvortsewich E.P., Milovskaya E.B. *J. Thermal Anal.*, **6**, 53 (1974).
20. Babichev A.P., Babushkina N.A., Bratkovskii A.M. *Fizicheskie velichiny* (Physical Properties)(Moscow: Energoatomizdat, 1991).
21. Chase M.W. *NIST-JANAF Thermochemical Tables* (Washington: Amer. Chem. Soc., 1998).
22. Paradis P.-F., Rhim W.-K. *J. Chem. Thermod.*, **32**, 123 (2000).
23. Ho C.Y., Powell R.W., Liley P.E. *J. Phys. Chem. Refer. Data*, **1**, 279 (1972).
24. Gorskii V.V., Shtyrya A.S. *Inzh.-Fiz. Zh.*, **49**, 374 (1985).
25. Ishi J., Kimura T. *Metrologia*, **5**, 50 (1969)
26. Zheng Y.W., Luk'yanchuk B.S., Lu Y.F., Song W.D., Mai Z.H. *J. Appl. Phys.*, **90**, 2135 (2001).
27. Arnold N. *Appl. Surf. Sci.*, **208-209**, 15 (2003).
28. Dobler V., Oltra R., Boquillon J.P., Mosbacher M., Boneberg J., Leiderer P. *Appl. Phys. A*, **69**, S335 (1999).